# Ordered Helium Trapping and Bonding in Compressed Arsenolite: Synthesis of As4O6·2He

*Juan Ángel Sans,\* Francisco Javier Manjón, Catalin Popescu, Vanesa Paula Cuenca-Gotor, Oscar Gomis, Alfonso Muñoz, Plácida Rodríguez-Hernández, Julia Contreras-Garcia, Julio Pellicer-Porres, Andre Luis de Jesus Pereira, David Santamaría-Pérez, and Alfredo Segura*

### Angle-dispersive X-ray diffraction (XRD) measurements under pressure

Highly pure arsenolite ($As_4O_6$) powder (99.999%) was commercially obtained from Sigma-Aldrich Company. High-pressure angle-dispersive XRD experiments at room temperature up to pressures between 15 and 30 GPa were conducted in a membrane-type diamond anvil cell (DAC) using commercial powder crushed in a mortar with a pestle to obtain a micron-sized powder. Measurements were performed with silicone oil (Rhodorsil 47V1000), methanol-ethanol (4:1 ratio) mixture, or He gas as quasihydrostatic pressure transmitting medium (PTM) and also without any PTM. Pressure inside DAC was estimated from the equation of state (EOS) of copper.[S1] Experiments were performed at the BL04-MSPD beamline of ALBA synchrotron with an incident monochromatic wavelength of 0.4246 Å focused to 20 x 20 $\mu m^2$.[S2] Pinhole of 50 $\mu m$ was used to clean the x-ray beam tail. Images covering a 2θ range up to 20° were collected using a SX165 CCD located at 240 mm from sample. One-dimensional diffraction profiles of intensity as a function of 2θ were obtained by integration of observed intensities with Fit2D software.[S3] Lattice parameters of powder XRD patterns were obtained by Rietveld refinements performed using GSAS program package.[S4,S5] Interatomic distances were extracted thanks to VESTA software.[S6]
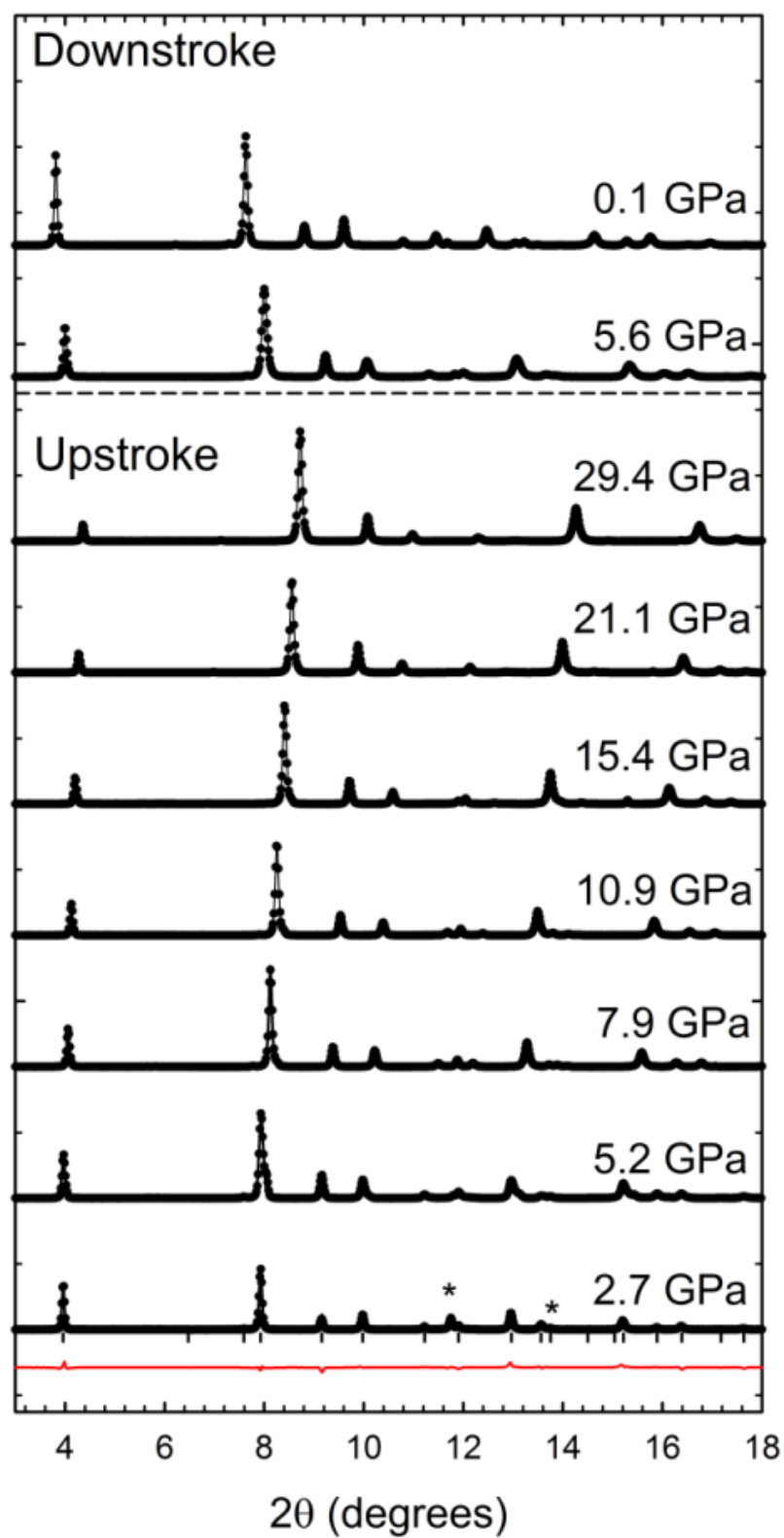
High-quality XRD patterns of arsenolite under compression using helium, (4:1) methanol-ethanol mixture and silicone oil as PTM and without PTM are displayed in Fig. S1. A progressive increase of the angle for all diffraction peaks of the cubic structure with increasing pressure is observed, as expected for a decrease in the unit cell volume under compression. Absence of new peaks at high pressure clearly indicates that no phase transition occurs along the pressure range studied. In the experiment with silicone oil, the increase of the intensity of the (200) Bragg peak and the decrease of the relative intensity of the peak corresponding to the lowest angle (111) reveal an increase of preferential orientation along the c-axis with increasing pressure. This preferential orientation has been considered during the Rietveld refinement by the addition of the spherical harmonics preferential orientation coefficients giving a texture index of 1.8-2.0, which is considered an intermediate value between 1 (no texturized) and 3 (strongly texturized). This feature is not observed in the rest of the experiments using He, (4:1) methanol-ethanol as PTM or without PTM. Furthermore, $As_4O_6$ compressed with (4:1) methanol-ethanol mixture, silicone oil and without PTM reveal the appearance of a progressive pressure-induced amorphization (PIA). On the contrary, arsenolite compressed with He shows no evidence of PIA up to the maximum pressure reached (29.4 GPa), even though there is a small increase of the width of the Bragg peaks at the highest pressures, likely due to a partial loss of hydrostaticity.

Rietveld refinement performed in the experimental XRD patterns of arsenolite allowed us to obtain the evolution of the lattice parameter and the Wyckoff sites of As and O with pressure. The evolution of the compressibility of the lattice parameter is equivalent to the EOS since it is a cubic structure. The experimental EOS of $As_4O_6$ compressed with different PTM and the comparison with the theoretically simulated compression curve of arsenolite and of He-trapped arsenolite with He located either at *8a, 16c* or *16d* Wyckoff sites are displayed in Fig.
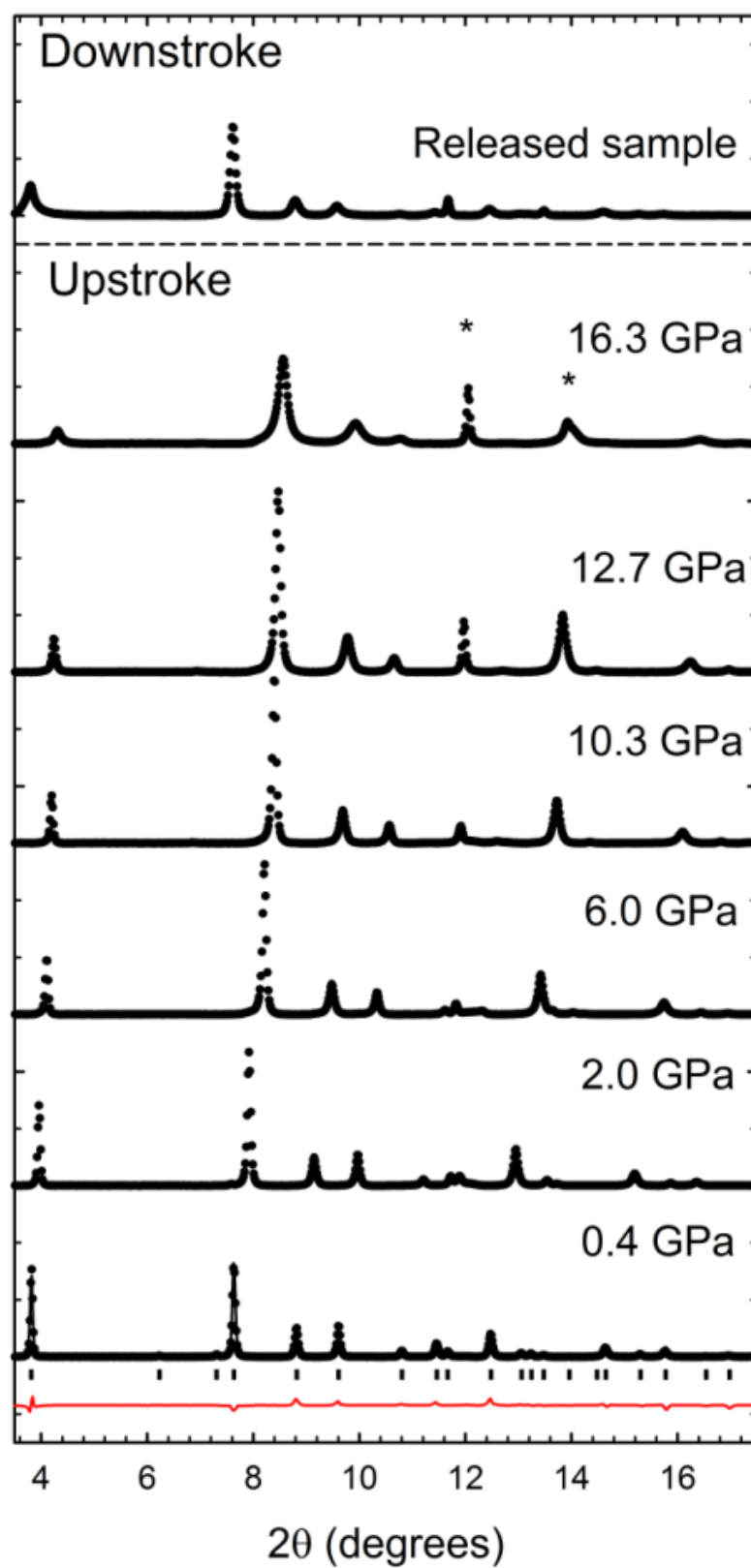
S2a. The experimental EOS obtained in the experiments using no PTM and silicone oil or methanol-ethanol as PTM yield a bulk modulus at ambient pressure around 7(2) GPa which is in good agreement with the theoretical EOS for arsenolite. However, the EOS of arsenolite compressed with He (using data above 5 GPa) yields a bulk modulus at ambient pressure of 4(2) GPa (see Table S1). This result is a little bit surprising since we expected a larger value of the bulk modulus of He-trapped arsenolite than the one obtained in bare arsenolite. This discrepancy could be an artifact due to the lack of experimental data of He-trapped $As_4O_6$ at low pressures (He exits *16d* sites below 3 GPa) since data at low pressures strongly influence the obtained value of the bulk modulus at ambient pressure. In order to stress the extraordinary small arsenolite's bulk modulus, its bulk modulus is compared to those of other sesquioxides of group-15 elements (see Table S2).
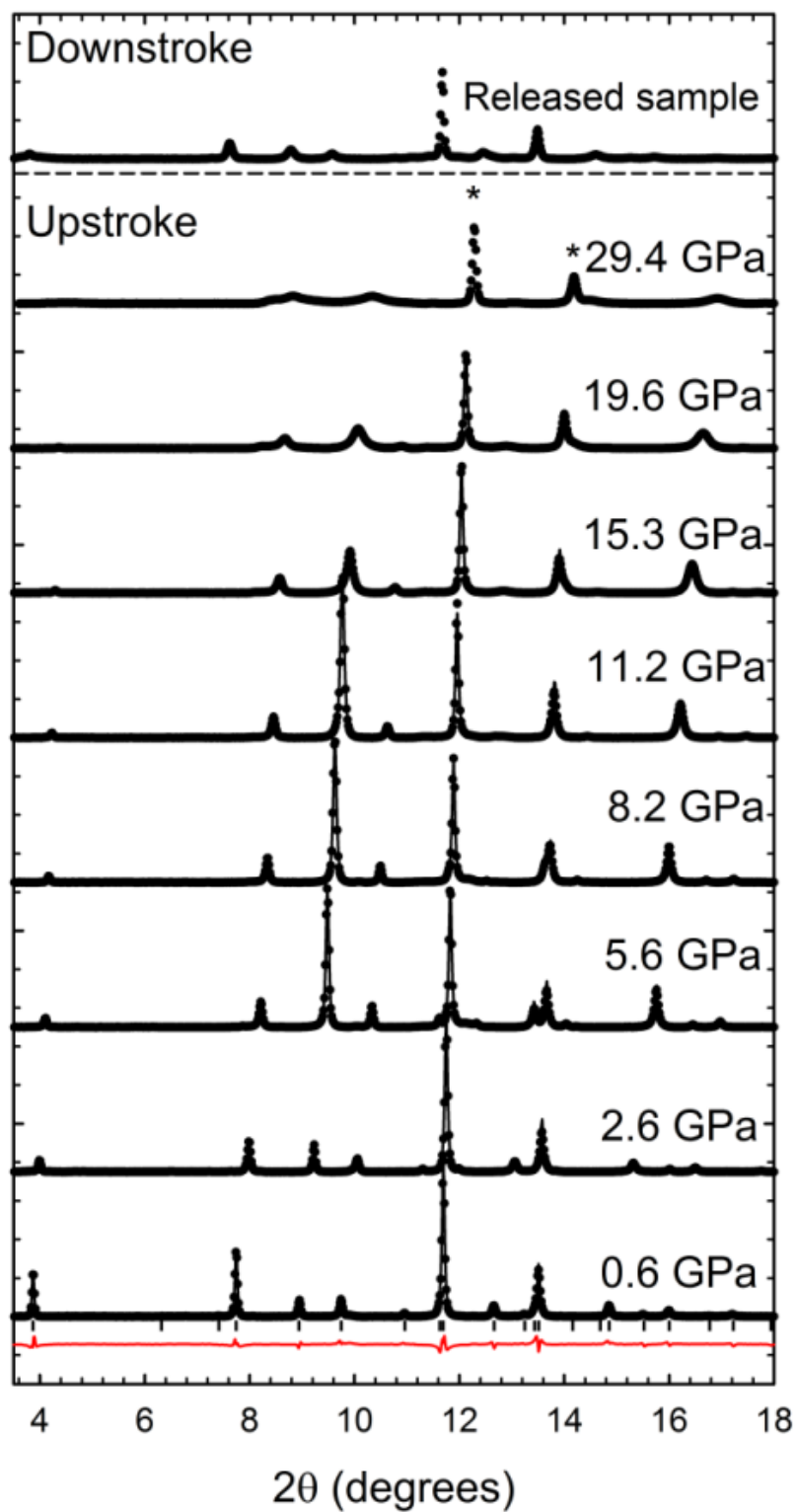
Evolution under pressure of the experimental and theoretical atomic coordinates of As and O is presented in Fig. S2b. Good agreement is found between experiments and theoretical curves for As Wyckoff sites, but a larger discrepancy is found for O Wyckoff sites. This result is due to the difficulty to accurately obtain the atomic position of light elements from Rietveld refinement of XRD data.

**b**

Downstroke

Released sample

Upstroke

16.3 GPa

*
*

12.7 GPa

10.3 GPa

6.0 GPa

2.0 GPa

0.4 GPa

2θ (degrees)

4

**C**



Downstroke

Released sample

Upstroke

*

*29.4 GPa

19.6 GPa

15.3 GPa

11.2 GPa

8.2 GPa

5.6 GPa
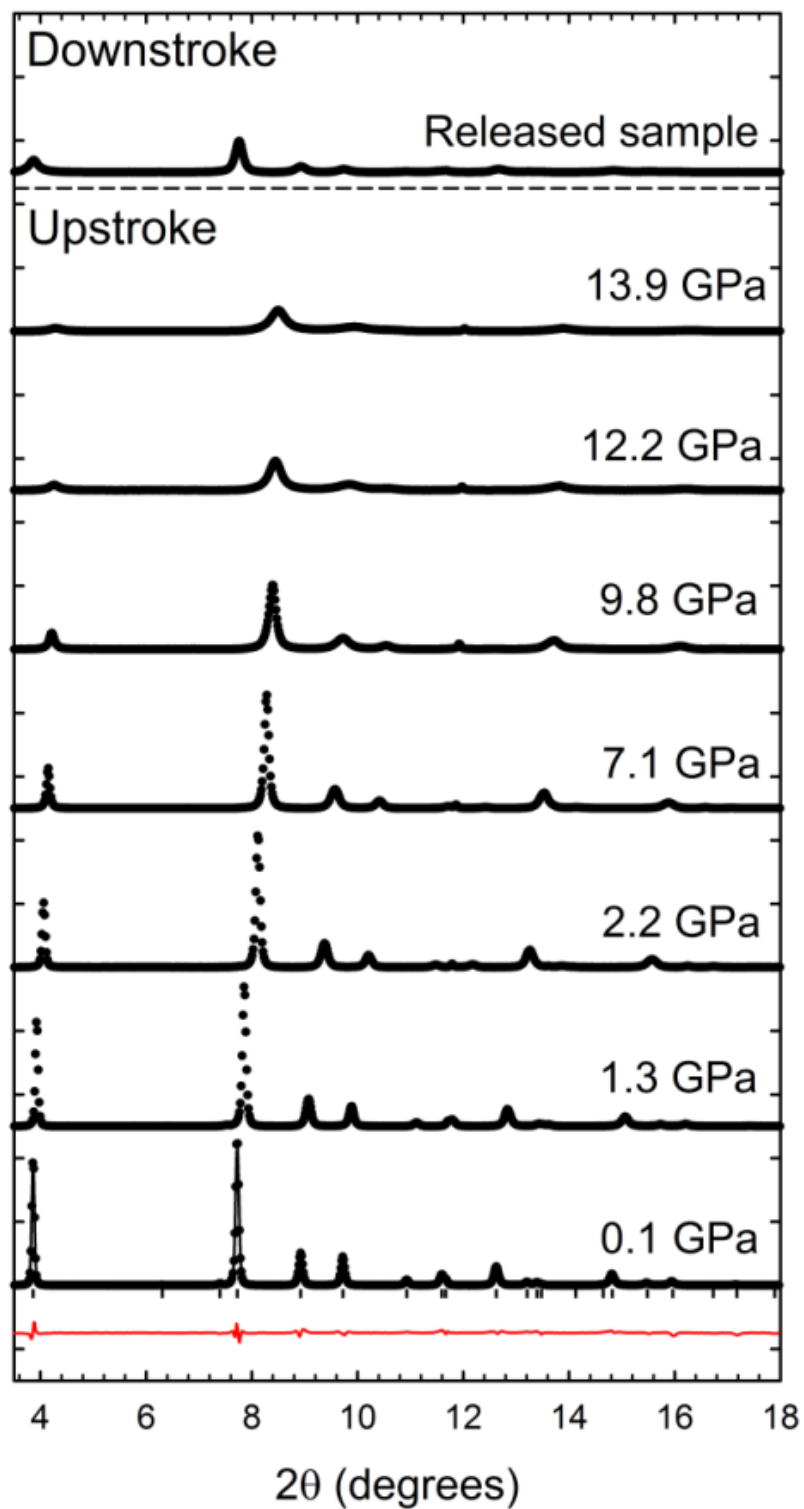
2.6 GPa

0.6 GPa

2θ (degrees)

**d**



FIG. S1. Experimental XRD patterns (vertically shifted for the sake of clarity) of arsenolite compressed with: a) helium; b) methanol-ethanol mixture; c) silicone oil and d) no PTM. Asterisks correspond to peaks of Cu. Red lines correspond to the residuals of the Rietveld

refinement at low pressures. Vertical ticks correspond to the position of the Bragg peaks included in the refinement.
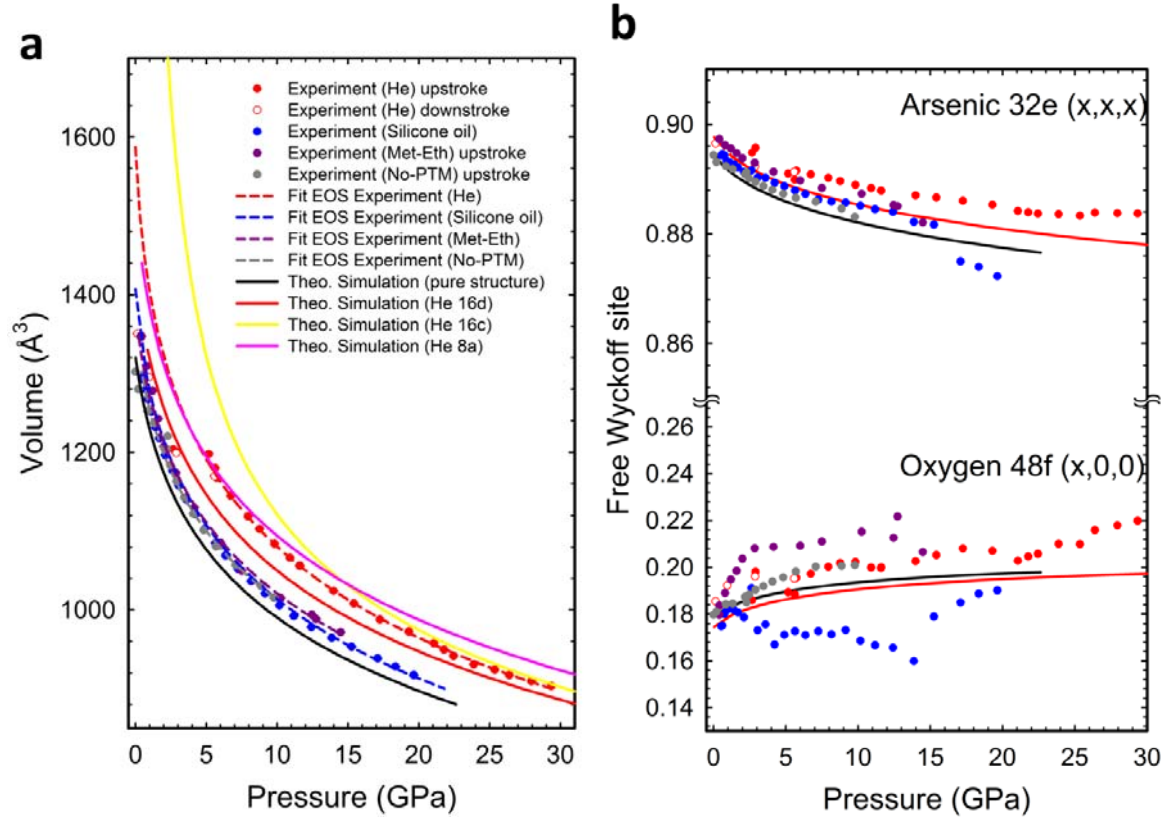


FIG. S2. EOS and evolution of atomic positions of arsenolite under pressure. a) Experimental and theoretically simulated EOS under different conditions. b) Pressure dependence of the free Wyckoff coordinates of As and O atoms. Grey, blue, purple, and red correspond to data of arsenolite compressed without PTM, with silicone oil, with methanol-ethanol mixture and with He, respectively. Black (red) solid line corresponds to theoretical data of pure (He-inserted at *16d* sites) arsenolite. Yellow (pink) solid line corresponds to theoretical data of arsenolite with He inserted at *16c* (*8a*) sites.

Table S1. Experimental and theoretical EOS of arsenolite

|  | $V_0$ [Å$^3$] | $B_0$ [GPa] | $B_0$' |
|---|---|---|---|
| Experimental (He)[a] | 1587(26) | 4(2) | 12.9 |
| Experimental (Sil. Oil) | 1407(2) | 6(1) | 12.9 |
| Experimental (Met-Eth) | 1385(15) | 7(2) | 12.9 |
| Experimental (No-PTM) | 1361(20) | 7(2) | 12.9 |
| Theo. Sim. (He 16d) | 1444(5) | 6.4(4) | 12.9 |
| Theo. sim. (pure) | 1331(2) | 7.6(3) | 12.9(3) |

[a] Data fitted above 5 GPa.

7

Table S2. EOS of different group-15 sesquioxides

| | $V_0$ [Å$^3$] | $B_0$ [GPa] | $B_0'$ |
|---|---|---|---|
| Pure-As$_2$O$_3$ (arsenolite)[a] | 1361(20) | 7(2) | 12.9 |
| As$_2$O$_3$ (claudetite)[b] | 308(2) | 18(2) | 3.5(5) |
| Sb$_2$O$_3$ (senarmontite)[c] | 1386(5) | 16.5(2) | 13.5 |
| α-Bi$_2$O$_3$ (bismite)[d] | 329(1) | 85.4(5) | 2.6(5) |
| β-Bi$_2$O$_3$ (beta-phase)[e] | 338.2(5) | 34(5) | 8(5) |
| β-Ga$_2$O$_3$ (beta-phase)[f] | 209 | 202(7) | 2.4(6) |
| In$_2$O$_3$ (Bixbyite)[g] | 64.28(13) | 184(10) | 4.0 |
| Tl$_2$O$_3$ (Bixbyite)[h] | 1170.6(1) | 147(13) | 5(2) |

[a] This work; [b] Ref. [S7]; [c] Ref. [S8]; [d] Ref. [S9]; [e] Ref. [S10]; [f] Ref. [S11]; [g] Ref. [S12]; [h] Ref. [S13]

Lattice parameters and atomic Wyckoff positions obtained from Rietveld refinement allows calculating the experimental pressure dependence of intramolecular (internal) and intermolecular (external) As-As and As-O distances (see Fig. S3). Again, a good agreement is found between experimental and theoretical data for both distances except for As-O distances in the experiment with silicone oil. A slight shift of the atomic positions for As and O, but with the same pressure dependence, is theoretically predicted when He is located at *16d* sites of arsenolite and indeed experimentally observed when He is used as PTM. The compression of the experimental external and internal As-O distances with the different PTM used is less affected with the inclusion of He in *16d* sites than As-As distances (in good agreement with theoretical calculations). Internal As-As distance corresponds to the distance between As cations inside the tetrahedron of the cage-like molecular unit, while external As-As distance corresponds to the minimum distance between As atoms of two neighboring cages. In pure As$_4$O$_6$ under compression, the external As-As distance tends to decrease monotonously (due to the closing of the gap between As$_4$O$_6$ molecules), whereas the internal As-As distance tends to slightly increase. Around 20 GPa, both internal and external As-As distances become nearly equal (external As-As distance is less than 3% longer than the internal As-As distance at 15 GPa when PIA starts to occur). Our calculations could suggest that the similarity of external and internal As-As distances above 15 GPa results in strong intermolecular interactions that make the cubic structure of arsenolite unstable. Nevertheless, He trapping in arsenolite above 3 GPa leads to a considerably increase of the external As-As distance (see the jump in Fig. S2a), thus avoiding the intermolecular interactions which turn the crystalline structure of arsenolite unstable. This feature allows to explain the stability of arsenolite beyond 30 GPa when compressed with He (the experimental external As-As distance is still 6% larger than the internal As-As distance at 30 GPa).
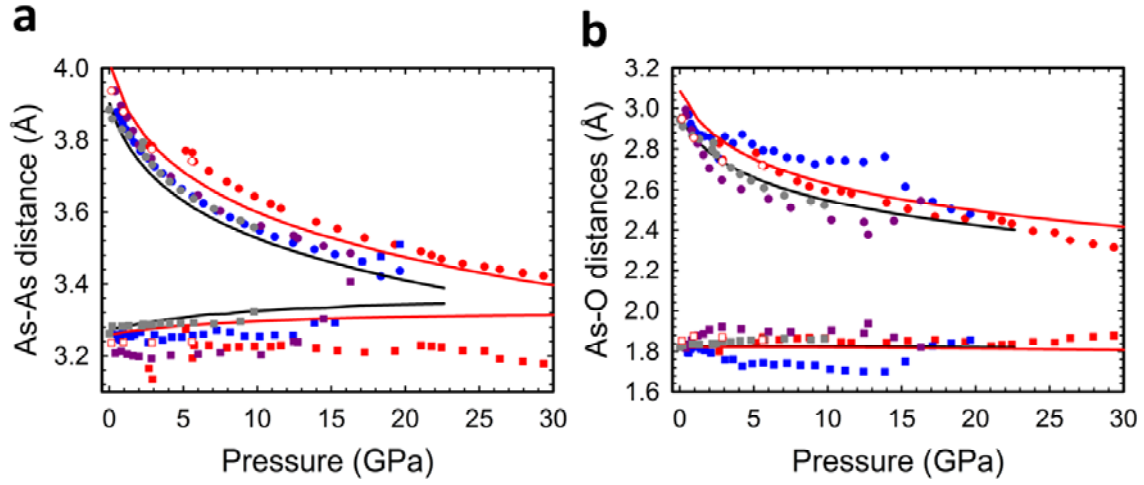
FIG. S3.  Pressure dependence of interatomic distances in arsenolite. Compression of the shortest interatomic distances belonging to the same molecular unit (squares) and different molecular units (circles): a) arsenic-arsenic and b) arsenic-oxygen. Grey, blue, purple, and red correspond to experimental data of arsenolite compressed without PTM, with silicone oil, with (4:1) methanol-ethanol mixture and with He, respectively. Black (red) solid line corresponds to theoretical data of pure (He-inserted at *16d* sites) arsenolite.
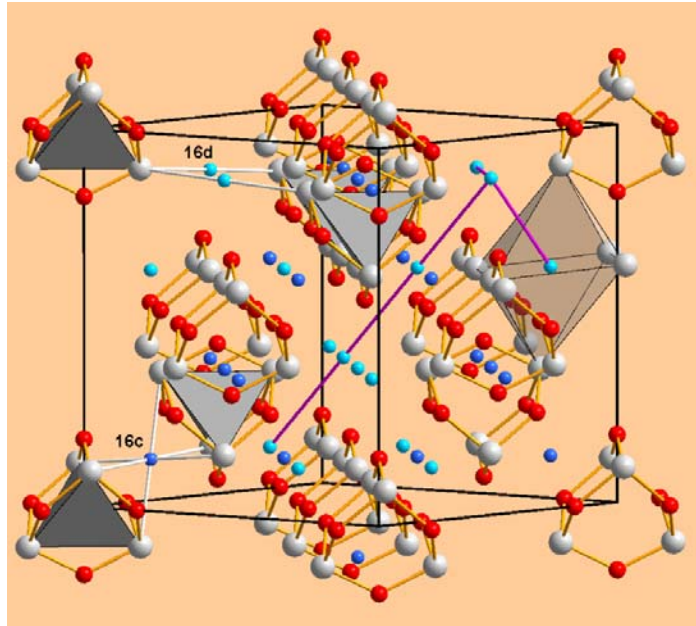


FIG. S4.  He-trapped arsenolite with He inserted into the two possible Wyckoff sites (16c and 16d). Big gray balls, medium-size red balls and small dark and light blue balls represent As, O, He(16c) and He(16d) atoms, respectively. Pink lines correspond to 3D diffusion paths for He along 16d sites.

*Raman scattering (RS) measurements under pressure*

High-pressure RS measurements at room temperature were performed in a backscattering geometry using a Horiba Jobin-Yvon LabRam HR UV spectrometer in combination with a thermoelectrically-cooled multichannel CCD detector (resolution below 2 cm$^{-1}$). RS spectra of arsenolite powder inside a DAC were excited either with 532.0 or 632.8 nm laser lines and laser power below 10 mW up to pressures between 12 and 22 GPa. RS measurements were performed with the same PTM as XRD measurements except for silicone oil. A few ruby balls of about 2 μm in diameter evenly distributed in the pressure chamber were employed as a pressure sensor.[S14] RS measurements were analyzed by fitting Raman peaks with a Voigt profile fixing the Gaussian line width (1.6 cm$^{-1}$) to the experimental setup resolution.[S15]

High-quality RS spectra of arsenolite under compression using helium, (4:1) methanol-ethanol mixture as PTM and without PTM are displayed in Fig. S5. A progressive shift of the Raman-active mode frequencies of all peaks of the cubic structure with increasing pressure is observed. Absence of new peaks at high pressure clearly indicates that no phase transition occurs along the pressure range studied. Only splitting of some modes is observed in samples compressed without PTM. These results and those obtained for arsenolite compressed with the methanol-ethanol mixture are similar to those already reported using CsI as PTM.[S16] Furthermore, many Raman modes, especially in the experiments without PTM and with the methanol-ethanol mixture, undergo a progressive asymmetric broadening above 10 GPa. This broadening is likely caused by the increase of intermolecular interactions; i.e., the increase of interactions among $As_4O_6$ cages, which finally results in the onset of PIA above 15 GPa. No such broadening of Raman modes is observed in the experiment performed with He up to 30 GPa.

Splitting and broadening of several Raman modes above 3-6 GPa (depending on the PTM used) are observed and attributed to the strong intermolecular interactions of compressed arsenolite. The different features observed in RS measurements depending on the PTM used can be explained by the different intermolecular interactions, related to external As-As and As-O distances, taking place in arsenolite compressed with or without He.

The experimental pressure dependence of the frequencies of the first-order Raman-active modes measured (only the soft mode $E_{g2}$ has not been observed as it has occurred in previous measurements)[S16] when arsenolite is compressed without PTM or with a PTM different from He is well reproduced by our theoretical calculations for $As_4O_6$ (Fig. S6). In the case of the arsenolite compressed with He as PTM, frequencies follow the same pressure dependence as in the previous experiments below 3 GPa. However, above 3 GPa almost all Raman modes suffer a small shift in frequency which is consistent with a volume increase at around 3 GPa: for modes with a positive pressure coefficient the shift is negative and vice versa. Additionally, some Raman-active modes of arsenolite show a completely different behavior when compressed with He above 3 GPa due to the incorporation of He in *16d* sites. Above this pressure, it is possible to observe a change of the phonon anticrossing affecting $T_{2g}^3$ and $T_{2g}^4$ modes corresponding to As-O bending modes. These two $T_g$ modes undergo a phonon anticrossing around 4.5 GPa when (4:1) methanol-ethanol mixture is used as PTM in good agreement with our lattice dynamics calculations of $As_4O_6$ and similar results can be observed in the experiment without PTM (Fig. S6). However, they shift apart above 3 GPa when arsenolite is compressed with He, thus resulting in a delay of the phonon anticrossing up to 11 GPa, which is nicely described by our theoretical calculations including He in *16d* Wyckoff sites (Fig. S6c). The incorporation of He at *16d* sites does not result in new Raman-active modes, but it results in two new infrared active modes whose frequencies are close to the $A_{1g}^1$

mode. Detailed analysis of Raman data with the different PTM are out of the scope of the present paper.
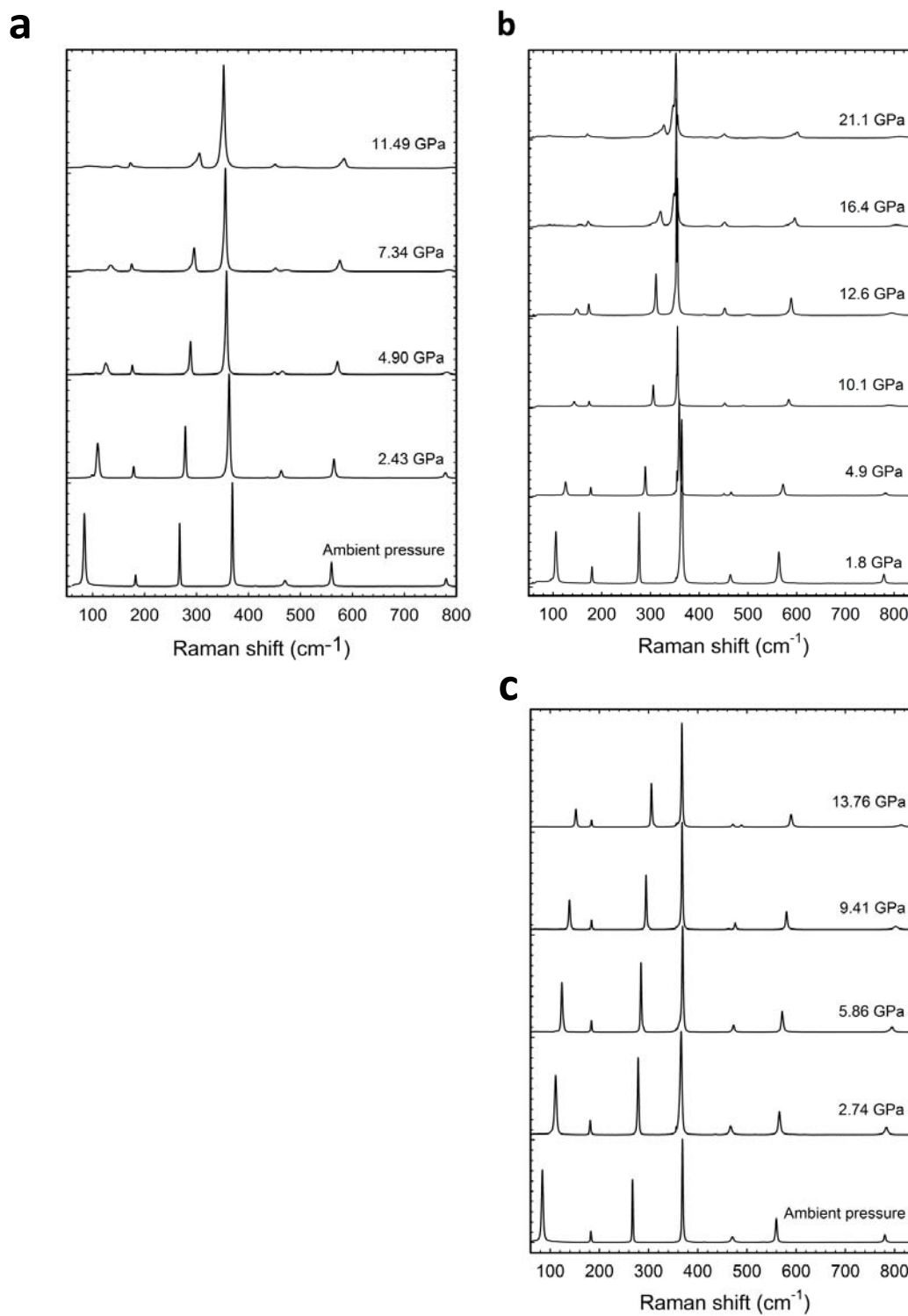
**a**



**b**



**c**

FIG. S5. RS spectra at selected pressures of arsenolite compressed with different PTM: a) no PTM; b) (4:1) methanol-ethanol mixture; and c) helium. RS spectra are vertically shifted for the sake of clarity.
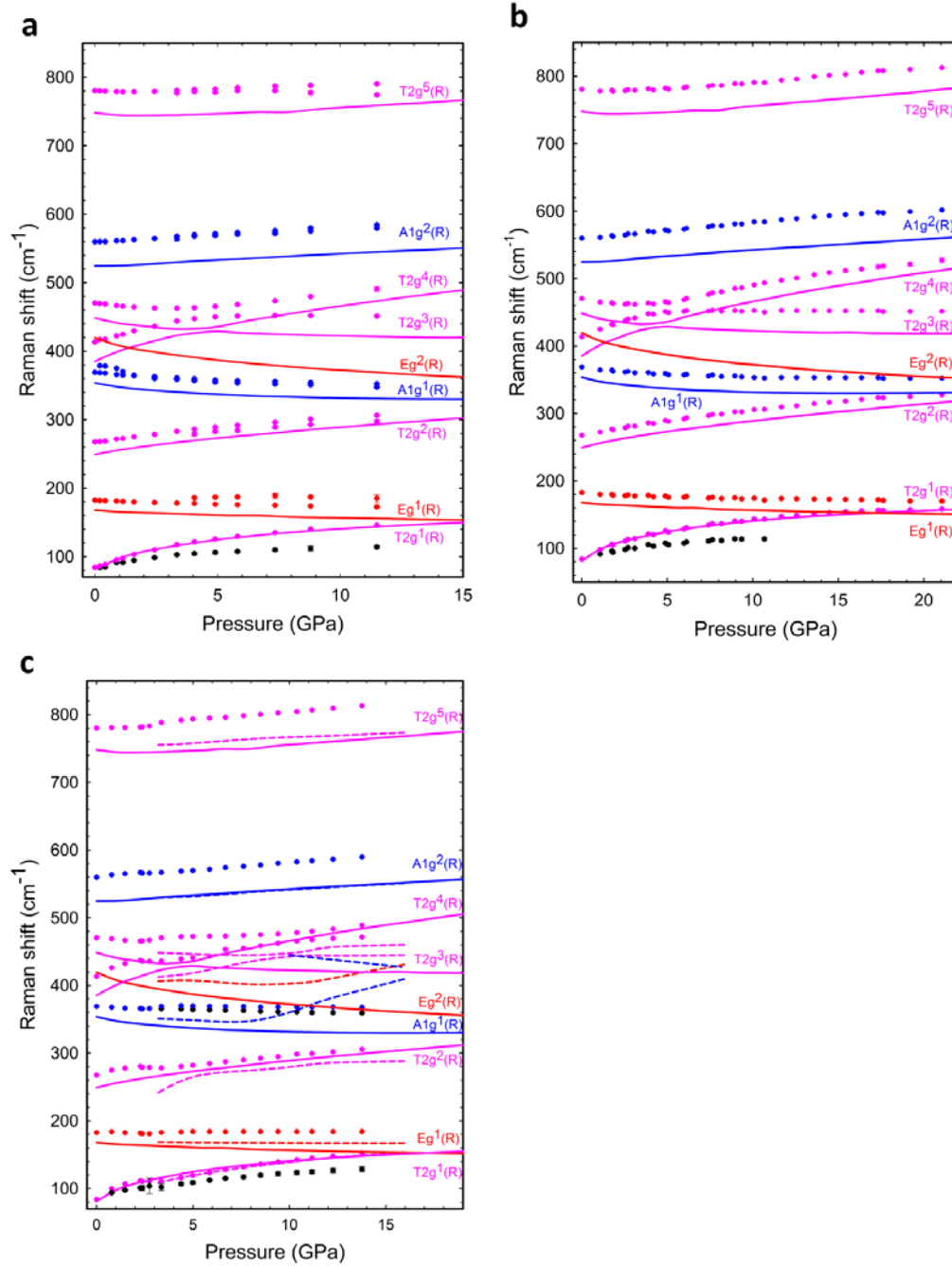


FIG. S6. Experimental (symbols) and theoretical (lines) pressure dependence of first-order Raman-active mode frequencies of arsenolite compressed with different PTM: a) no PTM; b) (4:1) methanol-ethanol mixture; and c) helium. Solid and dashed lines correspond to calculations of pure arsenolite and arsenolite with He-inserted at *16d* sites, respectively.

## Theoretical calculations

*Ab initio* total-energy calculations of arsenolite ($As_4O_6$) were performed within the framework of density functional theory (DFT).[S17] Vienna *Ab initio* Simulation Package (VASP) was used to carry out calculations with the pseudopotential method and the projector augmented wave (PAW) scheme, which replace the core electrons, make smoothed pseudovalence wave functions and take into account the full nodal character of the all-electron charge density in the core region.[S18] Exchange and correlation term was computed through PBE for solids prescription.[S19] Lattice-dynamics calculations at the zone center (Γ point) of the Brillouin zone were performed using the direct force constant approach.[S20] The elastic constants can be obtained by computing the macroscopic stress for a small strain with the use of the stress theorem.[S21] In the present work, we have performed the evaluation of the elastic constants of arsenolite as implemented in the VASP package.[S22] Hereafter, we will show that a new compound is formed ($As_4O_6 \cdot 2He$) when He is trapped at 16d sites. Therefore, hereafter the notation $As_4O_6$ and $As_4O_6 \cdot 2He$ is used to distinguish calculations in both compounds.
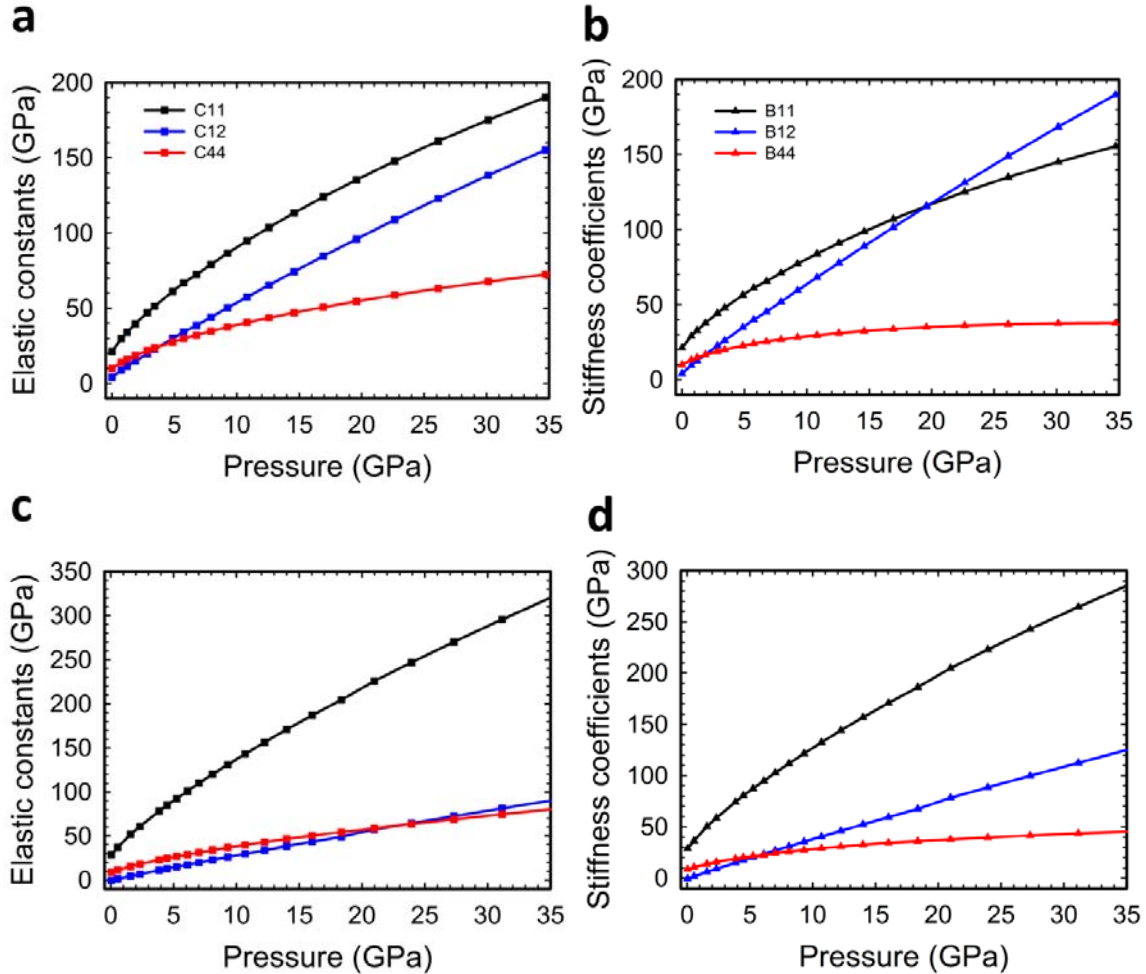


13

FIG. S7. Pressure dependence of the theoretical elastic constants and elastic stiffness coefficients of $As_4O_6$ and $As_4O_6·2He$. Elastic constants $C_{11}$, $C_{12}$, and $C_{44}$ of: a) $As_4O_6$; b) $As_4O_6·2He$. Elastic stiffness coefficients $B_{11}$, $B_{12}$, and $B_{44}$ of: c) $As_4O_6$; d) $As_4O_6·2He$.

Theoretical calculations have allowed us to obtain the evolution of the three independent elastic constants ($C_{11}$, $C_{12}$ and $C_{44}$) of cubic $As_4O_6$ and $As_4O_6·2He$ as a function of pressure (see Fig. S7). From the pressure dependence of the elastic constants, the pressure dependence of the elastic stiffness coefficients ($B_{11}$, $B_{12}$ and $B_{44}$) can be calculated (see Fig. S7)[S23] and defined as:

$$B_{11}=C_{11}-P; \quad B_{12}=C_{12}+P; \quad B_{44}=C_{44}-P$$

Once the elastic stiffness constants of a material in a given structure are known as a function of pressure the mechanical stability of the structure at high pressures can be evaluated by means of the generalized Born stability criteria.[S24,S25] For the mechanical stability of a cubic structure these criteria are:

$$M_1=B_{11} + 2B_{12}>0; \quad M_2=B_{11}-B_{12}>0; \quad M_3=B_{44}>0$$

The mechanical stability of $As_4O_6$ and $As_4O_6·2He$ can be discussed by the inspection of the generalized Born stability criteria plotted in Fig. S8. A Born instability in arsenolite due to the violation of the $M_2$ criterion occurs at 19.7 GPa; i.e., at a pressure close to that experimentally observed for the onset of PIA in our HP-XRD measurements using no PTM or using a PTM different from He. On the other hand, no mechanical instability is observed in $As_4O_6·2He$ even at 30 GPa in good agreement with our experimental results.
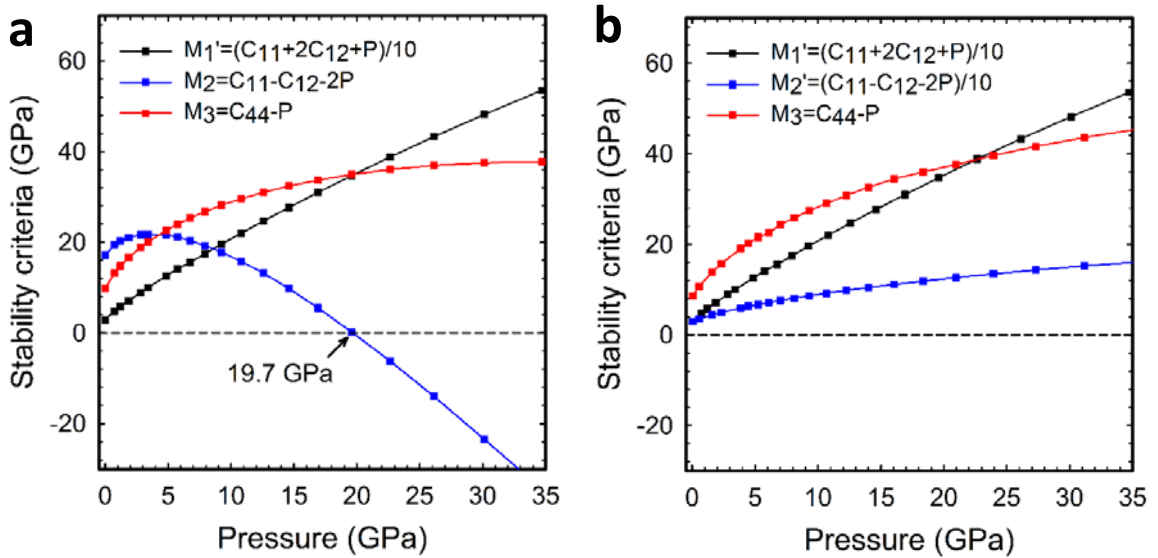


FIG. S8. Generalized Born criteria for mechanical stability under hydrostatic pressure in $As_4O_6$ (a) and $As_4O_6·2He$ (b).

Theoretical calculations of the electronic band structure of $As_4O_6 \cdot 2He$ shows the projected orbital distribution along the conduction and the valence band at 14 and 31 GPa (Fig. S9). The most relevant result is how He $1s$ orbitals, located deep in the valence band (red lines), behave under compression. The shape and evolution of their contribution evidences that they constitute bonding and antibonding orbitals with $s$ orbitals of As and $p$ orbitals of O, respectively. Three features that clearly indicate the reaction of He with $As_4O_6$ are: i) a downward (upward) shift in energy of the bonding (antibonding) band with increasing pressure; ii) an increase of the bandwidth of both bands with increasing pressure; and iii) an
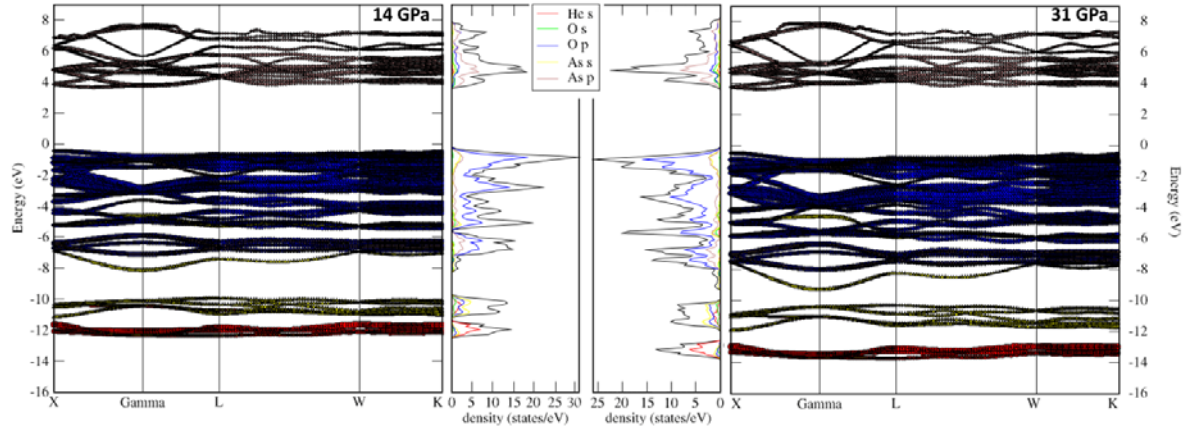


increase in the density of states of the antibonding band of He with increasing pressure. All these features allow us to conclude that there is a pressure-induced reaction of He with $As_4O_6$ resulting in the formation of $As_4O_6 \cdot 2He$.

FIG. S9. Pressure dependence of the band structure and projected distribution of orbitals of $He_2As_4O_6$ at 14 GPa (left) and 31 GPa (right).



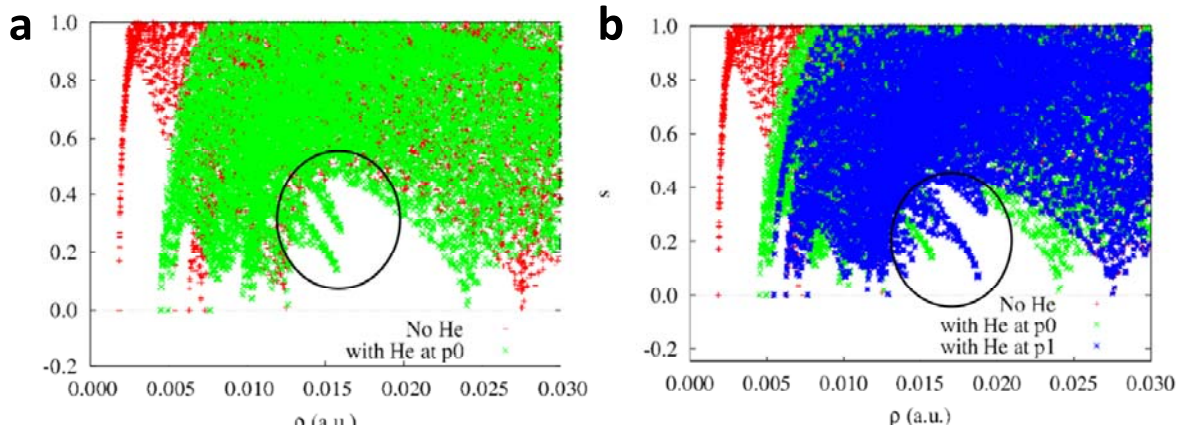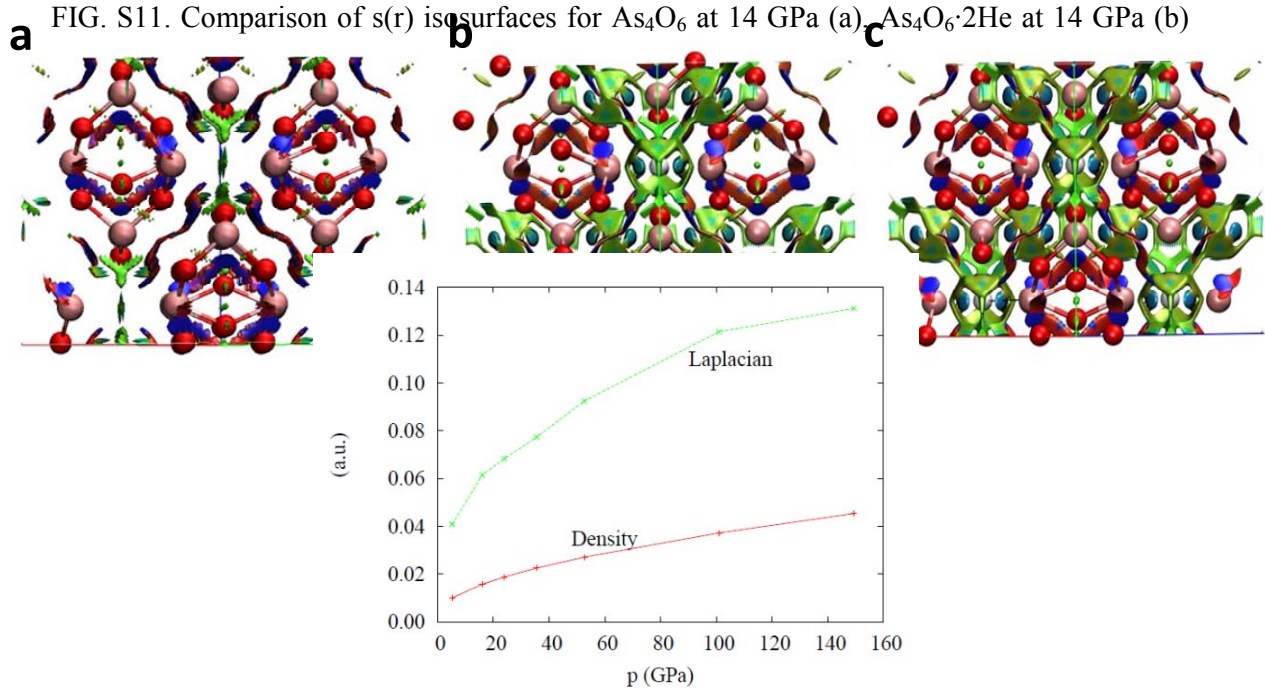FIG. S10. Comparison of s($\rho$) for $As_4O_6$ and $As_4O_6 \cdot 2He$ at 14 GPa (a) and at 31GPa (b).

In order to further show evidence of the interaction of He with arsenolite and the formation of $As_4O_6 \cdot 2He$ once He is trapped above 3 GPa, we have also conducted analysis of the electron density, $\rho$, using the *state-of-the-art* noncovalent interactions (NCI) index.[S26-S30] The recently disclosed NCI method relies on the relationship between the reduced density gradient s:[S26]

and the electron density $\rho$, to discriminate between various types of non-bonding interactions, such as attractive, van der Waals (vdW)-dispersive and repulsive ones. The two-dimensional plot of s *vs* the electron density $\rho$, gives rise to a plot where interactions appear as peaks. Their location in the diagram identifies the strength of the interaction, with stronger interactions appearing at higher densities.

These plots are shown in Fig. S10 for arsenolite ($As_4O_6$) and for $As_4O_6 \cdot 2He$ both at 14 and 31 GPa. The comparison of the structure upon inclusion of He atoms (Fig. S9a) enables to identify the new interactions as strongly attractive in nature. Moreover, when the evolution of the peaks is analyzed under pressure (Fig. S10b), we see that they are strengthened under pressure (they move to higher absolute values). NCI can be visualized by representing s isosurfaces, colored in order to reveal their nature and stregth: attractive interactions appear in blue turquoise, vdW interactions are revealed in green and steric clashes are colored in red. Within this representation, localized interactions appear as compact isosurfaces whereas delocalized ones appear as extended flat surfaces. This result is in contrast with the "charge-shift" bonding suggested by Rzepa for He atoms in stressed environments.[S31]

As expected for a noble gas, Fig S11 shows the appearance of van der Waals interactions around He atoms. However, unexpected localized interactions also make their appearance along the He-As interaction lines. In agreement with the s($\rho$) plot in Fig. S10, these interactions are strengthened (more intense in their blue color) with increasing pressure.

FIG. S11. Comparison of s(r) isosurfaces for $As_4O_6$ at 14 GPa (a) $As_4O_6 \cdot 2He$ at 14 GPa (b)

**a** **b** **c**



and $As_4O_6 \cdot 2He$ at 31 GPa (c).

FIG. S12. Pressure dependence of the electronic density and its Laplacian at the bond charge point of He-As.

In order to give quantitative details regarding the He-As interaction, we plot in Fig. S12 the pressure dependence of the electronic density and its Laplacian at the bond critical point of He-As. As observed, the interaction is small with an electronic density between 0.01 and 0.045 from 1 atm to 150 GPa. The small interaction between He and As atoms is different to the relatively strong "charge-shift" bonds recently predicted for He in stressed environments with electronic densities between 0.06 and 0.15 [S31].
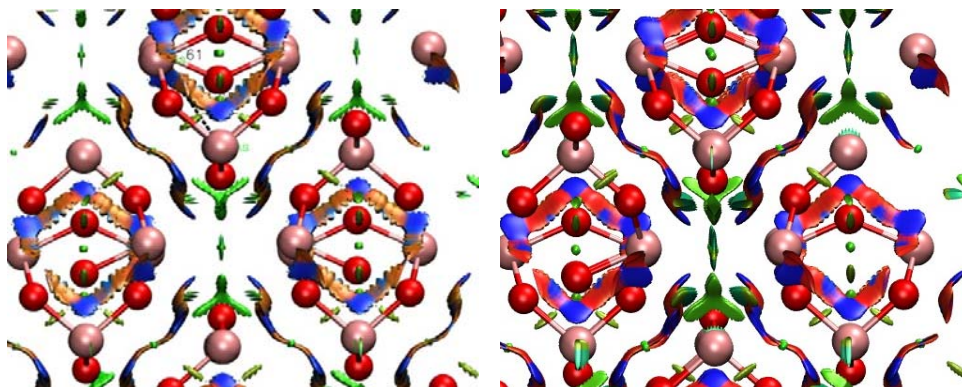


FIG. S13. Comparison of s(r) isosurfaces for $As_4O_6$ (left) at 5.7 GPa and for $As_4O_6$ at 14 GPa (right). Repulsive forces (red zigzag chains) between adamantane-type molecular units increase in intensity with increasing pressure.

Finally, we want to mention that theoretical calculations give support to the amorphization of arsenolite as due to repulsion between As atoms in neighbor molecular units. Fig. S13 shows a considerable increase of the repulsive forces between As atoms from 5.7 to 14 GPa which result in amorphization above 15-20 GPa.

[S1]    A. Dewaele, P. Loubeyre, M. Mezouar, *Phys. Rev. B*. 2014, 70, 094112.

[S2]    F. Fauth, I. Peral, C. Popescu, M. Knapp, *Powder. Diffr.* 2013, 28, S360.

[S3]    A. P. Hammersley, S. O. Svensson, M. Hanfland, A. N. Fitch, D. Hausermann, *High Pressure Res*. 1996, 14, 235.

[S4]    A. C. Larson, R. B. von Dreele, *LANL Report*. 1994, 86, 748.

[S5]    B. H. Toby, *J. Appl. Crystallogr*. 2001, 34, 210.

[S6]    K. Momma, F. Izumi, *J. Appl. Crystallogr*. 2011, 44, 1272.

[S7]    E. Soignard, S. A. Amin, Q. Mei, C. J.  Benmore, J. L. Yarger, *Phys. Rev. B*. 2008, 77, 144113.

[S8]    A. L. J. Pereira, L. Gracia, D. Santamaria-Perez, R. Vilaplana, F. J. Manjon, D. Errandonea, M. Nalin, A. Beltran, *Phys. Rev. B*. 2012, 85, 174108.

[S9]    A. L. J. Pereira, D. Errandonea, A. Beltran, L. Gracia, O. Gomis, J. A. Sans, B. Garcia-Domene, A. Miquel-Veyrat, F. J. Manjon, A.  Muñoz,  C. Popescu, *J. Phys.: Condens. Matter.* 2013, 25, 475402.

[S10]   A. L. J. Pereira, J. A. Sans, R. Vilaplana, O. Gomis, F. J. Manjon, P. Rodriguez-Hernandez, A. Muñoz, C. Popescu, A. Beltran, *J. Phys. Chem. C.* 2014, 118, 20545.

[S11]   D. Machon, P. F. McMillan, B. Xu, J. J. Dong, *Phys. Rev. B.* 2006, 73, 094125.

[S12]   B. García-Domene, J. A. Sans, O. Gomis, F. J. Manjón, H. M. Ortiz, D. Errandonea, D. Santamaría-Pérez, D. Martínez-García, R. Vilaplana, A. L. J. Pereira, A. Morales-García, P. Rodríguez-Hernández, A. Muñoz, C. Popescu, A. Segura, *J. Phys. Chem. C.* 2014, 118, 20545.

[S13]   O. Gomis, D. Santamaría-Pérez, J. Ruiz-Fuertes, J. A. Sans, R. Vilaplana, H. M. Ortiz, B. García-Domene, F. J. Manjón, D. Errandonea, P. Rodríguez-Hernández, A. Muñoz, M. Mollar, *J. App. Phys.* 2014, 116, 133521.

[S14]   M. K. Mao, J. Xu, P. M. Bell, *J. Geophys. Res.* 1986, 91, 4673.

[S15]   A. Debernardi, C. Urlich, M. Cardona, K. Syassen, *Phys. Status Solidi B.* 2001, 223, 213.

[S16]   A. Grzechnik, *J. Sol. State Chem.* 1999, 144, 416.

[S17]   P. Hohenberg, W.  Kohn, Phys. Rev. 1964, 136, 3864.

[S18]   P. E. Blo   chl, *Phys. Rev. B: Condens. Matter Mater. Phys*. 1994, 50, 17953.

[S19]   J. P. Perdew, A. Ruzsinszky, G. I. Csonka, O. A. Vydrow, G. E. Scuseria, L. A. Constantin, X. Zhou, K. Burke, *Phys. Rev. Lett.* 2009, 100, 136406.

[S20]  K. Parlinski, Z. Q. Li, Y. Kawazoe, *Phys. Rev. Lett*. 1997, 78, 4063.

[S21]  N. Chetty, A. Muñoz, R. M. Martin, *Phys. Rev. B*. 1989, 40, 11934.

[S22]  Y. Le Page, P. Saxe, *Phys. Rev. B*. 2002, 65, 104104.

[S23]  D. C. Wallace, *Thermoelastic theory of stressed crystals and higher-order elastic constants, in Solid State Physics*, Academic Press, USA 1970.

[S24]  M. Born, *I. Proc. Cambridge Philos. Soc.* 1940, 36, 160.

[S25]  J. Wang, S. Yip, S. R. Phillpot, D. Wolf, *Phys. Rev. Lett*. 1993, 71, 4182.

[S26]  E. Johnson, S. Keinan, P. Mori-Sánchez, J. Contreras-García, A. Cohen and W. Yang, *J. Am. Chem. Soc*. 2010, 132, 6498.

[S27]  J. Contreras-García, E. Johnson, S. Keinan, R. Chaudret, J. Piquemal, D. Beratan and W. Yang, *J. Chem. Theory Comput*. 2011, 7, 625.

[S28]  J. Contreras-García, W. Yang and E. Johnson, *J. Phys. Chem. A* 2011, 115, 12983.

[S29]  A. Otero-de-la-Roza, J. Contreras-Garcia, E. R. Johnson, *Phys. Chem. Chem. Phys.* 2012, 14, 12165.

[S30]  G. Saleh, C. Gatti, L. Lo Presti, J. Contreras-Garcia, *Chem. Eur. J.* 2012, 18, 15523.

[S31]  H. S. Rzepa. Nat. Chem. 2, 390 (2010).